Proceedings of the Thirty-sixth (2026) International Ocean and Polar Engineering Conference **www.isope.org**
Orlando, Florida, USA, May 31-June 5, 2026

ISBN 978-1-880653-72-2; ISSN 1098-6189

Kelvin Wake Induced by an Improved Gaussian Pressure Distribution Based on High Order Spectral Method

*Pengju Bao, Yuan Zhuang, Decheng Wan**

Computational Marine Hydrodynamics Lab (CMHL), School of Ocean and Civil Engineering,
Shanghai Jiao Tong University, Shanghai, China
*Corresponding author

ABSTRACT

The Kelvin wake's persistent nature poses both detection risks and research value. This study develops an improved pressure distribution model to better represent the hull-induced disturbance on the free surface. The proposed formulation overcomes key limitations of the standard Gaussian distribution, particularly its strict symmetry and excessive smoothness at bow and stern regions, by introducing independent shape parameters that enable more accurate geometric representation of actual ship hulls. Implemented within the high order spectral (HOS) method, the model successfully generates dual wave systems and shows improved agreement in near-field surface elevation, providing enhanced capability for Kelvin wake simulation in open-sea conditions.

KEY WORDS: High Order Spectral method; Gaussian pressure distribution; Wide-area Kelvin wake.

INTRODUCTION

The movement of a vessel on the water surface is invariably accompanied by the generation of surface wakes behind it. Among these wakes, Kelvin wake is distinguished by its extensive propagation range and persistent nature. The characteristics of this wave system can be leveraged to inversely deduce key structural parameters of the vessel (Tunaley, 2003; Arnold-Bos, et al, 2007; Gomit, et al, 2014; Graziano, et al, 2016), which entails a risk of information disclosure. Consequently, research on ship wakes is of pivotal practical importance, both for fundamental hydrodynamic understanding and for critical maritime applications.

The simulation of Kelvin wakes is primarily addressed through potential flow theory or computational fluid dynamics (CFD). Due to the extensive nature of ship wakes, resolving a relatively complete wave system requires a computational domain of equivalent scale. While CFD offers high accuracy in localized regions, its application is constrained by boundary conditions, making it unsuitable for modeling wake evolution in open seas. Moreover, computational costs become prohibitively high as grid resolution increases. Traditional potential flow methods are relatively efficient for wave-related problems but still demand substantial computational resources for large domains.

The High Order Spectral (HOS) method, introduced by Dommermuth and Yue in 1987, leverages pseudo-spectral techniques and the Fast Fourier Transform (FFT), exhibiting exceptionally rapid convergence. Ducrozet et al. (2016) later developed the open-source code HOS-Ocean, which efficiently simulates nonlinear wave propagation in open seas. However, this implementation does not account for the presence of a vessel and thus cannot simulate the generation of surface wakes.

Many researchers have adopted a moving pressure distribution to approximate the hull's disturbance on the free surface, incorporating it into the dynamic free-surface boundary conditions (Yeung, et al, 2008; Rabaud and Moisy, 2013; Moisy and Dabaud, 2014; Colen and Kolomeysky, 2021; Lo, 2021; Paprota, 2023). This approach has enabled extensive investigation of Kelvin wake characteristics across multiple aspects, significantly advancing the understanding of such wakes. Among various models, the Gaussian pressure distribution has been widely employed due to its favorable mathematical properties. However, the standard Gaussian distribution represents an oversimplification that significantly deviates from the geometry of an actual ship hull. On one hand, its pressure center features a rounded peak that attenuates smoothly outward, which contrasts with the typically flatter bottom and more rectangular mid-body section of a submerged hull form. On the other hand, the Gaussian distribution is strictly symmetric and often employs identical decay rates in both the longitudinal and transverse directions. This does not reflect the reality of a ship hull, which typically has distinct stem and stern shapes, as well as side curvatures that differ from those at the bow and stern.

Furthermore, the influence of the decay coefficient within the exponential term of the Gaussian function appears ambiguous, as there seems to be no clear reference standard for determining its value. In studies (Moisy and Dabaud, 2014; Lo, 2021; Paprota, 2023) employing the Gaussian pressure distribution to investigate Kelvin wakes, different yet numerically close decay coefficients have been selected. Bao et al., (2025) have applied several such choices to the same hull and found that the impact on the far-field wave system is not significant. In the near field, the first one or two peaks and troughs exhibit a trend of increasing magnitude with the decay coefficient. Nevertheless, since the selected coefficients are similar, this difference remains subtle. Should the value of this coefficient become exceedingly large, whether the impact on the results would be significant remains an open question.

To overcome the aforementioned limitations, this study proposes a refined pressure distribution model derived from the standard Gaussian framework. The newly developed formulation incorporates adjustable parameters that enable the generation of diverse pressure distribution patterns, thereby providing a more accurate representation of the actual disturbance induced by a ship hull on the free surface.

NUMWRICAL METHODS

High Order Spectral Method

The High Order Spectral (HOS) method is founded upon potential flow theory, adhering to its fundamental assumptions of an incompressible, inviscid fluid and irrotational flow field. A right-handed Cartesian coordinate system is established with its origin located at the still water level and the positive z-axis directed vertically upward. When representing the horizontal directions, the x-axis is conventionally aligned with the primary direction of wave propagation, while the y-axis completes the orthogonal coordinate frame, i.e. $\boldsymbol{x} = (x, y)$. Following the theoretical framework established by Zakharov (1968), the surface velocity potential ϕ^s is introduced as the fundamental dynamic variable governing the nonlinear free surface boundary conditions.

$$\phi^s(\boldsymbol{x},t) = \phi(\boldsymbol{x},\eta,t) \tag{1}$$

Based on the assumptions that both the velocity potential ϕ and the surface elevation η are of order $O(\varepsilon)$, and that the wave steepness $\varepsilon = ka$ (where k denotes the wavenumber and a the wave amplitude), ϕ can be asymptotically expanded as a perturbation series. Furthermore, this potential is expanded as a Taylor series about the still water level ($z = 0$) and truncated at a consistent order M , leading to the following expression:

$$\begin{aligned}\phi^{m}(\boldsymbol{x},z,t) &= \sum_{n=1}^{\infty}\phi_n^{m}(t)\psi_n(\boldsymbol{x},z) \\ &= \sum_{n=0}^{\infty}\phi_n^{(m)}(t)\frac{\cosh\,|\boldsymbol{k_n}|(z+h)}{\cosh\,|\boldsymbol{k_n}|h}\exp(i\boldsymbol{k_n}\cdot\boldsymbol{x})\end{aligned} \tag{2}$$

Substituting these into the free surface boundary conditions yields the equations for η and ϕ^s :

$$\begin{aligned}&\eta_t + \nabla_x\phi^s\cdot\nabla_x\eta - (1+\nabla_x\eta\cdot\nabla_x\eta) \\ &-(1+\nabla_x\eta\cdot\nabla_x\eta)\left[\sum_{m=1}^{M-m}\sum_{k=0}^{M-m}\frac{\eta^k}{k!}\sum_{n=1}^{N}\phi_n^{m}(t)\frac{\partial^{k+1}}{\partial z^{k+1}}\psi_n(\boldsymbol{x},0)\right] = 0\end{aligned} \tag{3}$$

$$\begin{aligned}&\phi_t^s + g\eta + \frac{1}{2}\nabla_x\phi^s\cdot\nabla_x\phi^s \\ &-\frac{1}{2}(1+\nabla_x\eta\cdot\nabla_x\eta)\left[\sum_{m=1}^{M}\sum_{k=0}^{M-m}\frac{\eta^k}{k!}\sum_{n=1}^{N}\phi_n^{m}(t)\frac{\partial^{k+1}}{\partial z^{k+1}}\psi_n(\boldsymbol{x},0)\right]^2 + \frac{P}{\rho} = 0\end{aligned} \tag{4}$$

where the subscript t denotes the partial derivative with respect to time, and the differential operator ∇_x represents the spatial gradient. The gravitational acceleration is denoted by g , and the fluid density by ρ . The pressure term P is defined as relative pressure and is taken to be zero in the absence of free-surface disturbances; otherwise, it corresponds to a prescribed surface pressure distribution.

Pressure Distribution Term

To simulate the generation and evolution of Kelvin wakes, a pressure distribution term must be introduced into the free-surface boundary conditions to represent the ship-induced disturbance. Considering a vessel in steady, straight-ahead motion through calm water, the Kelvin wake reaches a fully developed state where ship motions except surge can be considered stationary for practical purposes. Under these conditions, oscillatory motions (such as heave and pitch) are either negligible or exert minimal influence on the wake characteristics. By approximating the moving ship's effect with the pressure field generated by its stationary counterpart, the fundamental form of this pressure distribution can be mathematically represented as follows:

$$P(x,y) = \rho g\cdot D(x,y) = \rho g\cdot D_s\cdot S(x,y) \tag{5}$$

where $D(x,y)$ denotes the local draft at various positions on the hull surface, which can be approximated by multiplying the maximum or mean draft by a shape factor $S(x,y)$. Due to its favorable mathematical properties, the Gaussian pressure distribution is widely adopted. Considering a standard two-dimensional Gaussian pressure function with a peak value of 1, the shape factor $S_2(x,y)$ can be expressed as:

$$S_2(x,y) = \exp\left(-\frac{1}{2}\left[\frac{(x-\mu_x)^2}{\sigma_x^2} + \frac{(y-\mu_y)^2}{\sigma_y^2}\right]\right) \tag{6}$$

where μ_x and μ_y represent the coordinates of the peak center of the shape factor, while σ_x and σ_y denote its spatial extents in the longitudinal and transverse directions, respectively. The distribution exhibits a bell-shaped curve, which is concentrated near its center. Furthermore, the characteristic bell-shaped profile of the standard Gaussian distribution may inadequately represent the box-like structural characteristics of certain hull forms. Drawing inspiration from the concept of the super-ellipse, the implementation of alternative exponential terms presents a viable alternative. If expressed in the form of a super-Gaussian distribution, Eq. (6) can then be rewritten as:

$$S(x,y) = \exp\left(-\frac{1}{2}\left[\frac{(x-\mu_x)^n}{\sigma_x^n} + \frac{(y-\mu_y)^n}{\sigma_y^n}\right]\right) \tag{7}$$

To preserve desirable mathematical properties of the distribution, it is generally recommended that the values of n be positive even integers. When $n = 2$, the formulation reduces to the standard Gaussian pressure distribution. For values of $n > 2$ (so called flat-top Gaussian distribution, here), the pressure profile becomes progressively more rectangular, thereby effectively representing the parallel middle-body characteristics typical of ship hulls. Consider the ship length L_s , beam B_s , if the shape dimensions at $1/a$ ($a > 1$ is a constant) in Eq. (7) are used to characterize the ship geometry, then (see Appendix A.):

$$\sigma_x = \frac{L_s/2}{(2\log(a))^{1/n}}, \qquad \sigma_y = \frac{B_s/2}{(2\log(a))^{1/n}} \tag{8}$$

Hence, one can then obtain the distribution expressed as Eq. (9):

$$S(x,y) = \exp\left(-\beta\left[\frac{(x-\mu_x)^n}{L_s^n} + \frac{(y-\mu_y)^n}{B_s^n}\right]\right) \tag{9}$$

where $\beta = 2^n \log(a)$ denotes the decay coefficient, a shape-governing parameter. When $n = 2$, $\beta = 4log(a)$, and a higher value of a leads to a more concentrated and pronounced pressure peak, whereas a lower value produces a broader and more gradual pressure distribution (Bao et al., 2025). The different values of a and n respectively govern the curvature steepness of the pressure distribution curve and the width range of the distribution, which is an inherent property of the mathematical expression. Observing Eq. (9), it is evident that it consists of the product of two exponential functions of similar form, one in x and the other in y, corresponding to the longitudinal and transverse directions, respectively. Then the shape factor $S(x, y)$, governing the pressure distribution profile, admits a separable form and can be expressed as the product of two independent functions, a longitudinal function $f(x)$ and a transverse function $g(y)$:

$$S(x,y) = f(x) \cdot g(y) \tag{10}$$

It is evident that the decay coefficient β exerts identical effects in both longitudinal and transverse directions, indicating that the Gaussian pressure distribution exhibits strict symmetry. This characteristic, however, significantly deviates from the actual hull geometry. To address this discrepancy, the adoption of distinct decay coefficients for longitudinal and transverse directions may be considered. Consequently, this study proposes a modified generalized Gaussian pressure distribution, which enables enhanced and diversified control over the pressure distribution morphology through parameter adjustments, as expressed in the following formulation:

$$S\ x,y\ = \exp(-\left[\beta_x\left(\frac{(x-\mu_x)}{L_s}\right)^{n_x} + \beta_y\left(\frac{(y-\mu_y)}{B_s}\right)^{n_y}\right]) \tag{11}$$

where $\beta_x = 2^{n_x}\log(a_x)$ and $\beta_y = 2^{n_y}\log(a_y)$ denote the longitudinal and transverse decay coefficients, respectively, while n_x and n_y represent the corresponding exponential factors in the longitudinal and transverse directions.

To achieve a more refined representation of the hull's bow-stern asymmetry, the decay coefficient β_x and the exponential factor n_x can be further decomposed into separate components for the bow and stern regions, as expressed in the following formulation:

$$S\ x,y\ = \exp(-\left[\beta_{xr}\left(\frac{(x-\mu_x)}{L_{sr}}\right)^{n_{xr}} + \beta_y\left(\frac{(y-\mu_y)}{B_s}\right)^{n_y}\right]) \tag{12}$$

$$q_{ir} = \begin{cases} q_{iF}, & for\ x_c < 0 \\ q_{iA}, & for\ x_c \geq 0 \end{cases} \tag{13}$$

where q_i is a quantity which could be β_x, a_x, n_x and L_s. A simplified configuration is considered where the bow and stern lengths are defined as L_{sF} and L_{sA} respectively, satisfying $L_{sF} + L_{sA} = L_s$, with the longitudinal center of gravity positioned at x_c. By independently adjusting the longitudinal decay coefficient β_x and exponential factor n_x for the forward (Fwd) and aft regions, the pressure distribution can be effectively tailored to represent the distinct geometrical characteristics of the bow and stern sections.

RESULTS

Effects of Shape Parameters on Pressure Distribution

In the proposed improved Gaussian pressure distribution model, the main adjustable parameters are centralized within the shape factor $S(x, y)$, specifically the decay coefficients β and exponent parameters n defined separately for longitudinal and transverse directions. Given the analogous nature of the longitudinal and transverse characteristics, the longitudinal pressure distribution is taken as an example to investigate the influence of parameter variations on the pressure profile. The corresponding shape factor is thus written as $S(x)$:

$$S\ x\ = \exp(-\beta\left(\frac{|x-\mu_x|}{L_s}\right)^{n_x}) \tag{14}$$

For clarity in the discussion, the center of the pressure distribution is fixed at the origin, i.e., $\mu_x = 0$. Various parametric configurations, as summarized in Tab. 1, are examined to illustrate their influence on the resulting pressure distribution shapes. To provide more intuitive geometric interpretation, the decay coefficient β is replaced by an equivalent peak ratio coefficient a. The reference case is the standard Gaussian pressure distribution employed by Lo (2021), which uses $\beta = 8$, corresponding to $a = 7.39$.

Tab. 1 Configuration combinations of different shape parameters.

Configuration 1: $n_x = 2$						
a	7.39	15	25	50	100	200
Configuration 2: $a = 7.39$						
n_x	2	4	6	8		
Configuration 3: $n_x = 4$						
a	7.39	15	25	50		

As shown in Fig. 1, overall, all distributions exhibit the characteristic bell-shaped form with smoothly rounded peaks. The pressure attenuates gradually from the peak toward both sides, with this decay trend intensifying as the coefficient increases. Consequently, the profile contracts inward and steepens significantly, thereby requiring a higher spatial resolution to adequately capture the increasingly sharp pressure gradient.

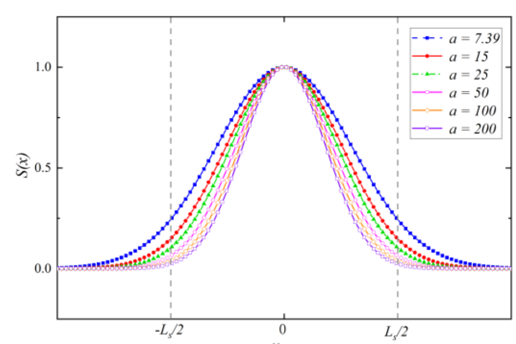

Fig. 1 A comparison of pressure distribution profiles under varying decay coefficients β while maintaining a fixed exponential factor $n_x = 2$ (configuration 1).

As shown in Fig. 2, compared to the standard Gaussian distribution

($n_x = 2$), increasing n_x results in significant morphological changes: the pressure profile transitions from a classical bell shape to a more plateau-like form with extended shoulders, effectively widening the distribution. This flattened top profile better represents the parallel middle body section of ship hulls, while the extended shoulders may potentially generate wave patterns analogous to bow and stern wave systems. All profiles with varying n_x intersect at the half-ship length ($L_s / 2$) position when a remains constant, precisely at the normalized elevation of $1/a$. Quantitative analysis reveals that larger n_x values produce more abrupt attenuation characteristics, with this parametric effect appearing more pronounced than that of β . This intensified spatial variation consequently demands enhanced grid resolution to adequately resolve the steep pressure gradients.

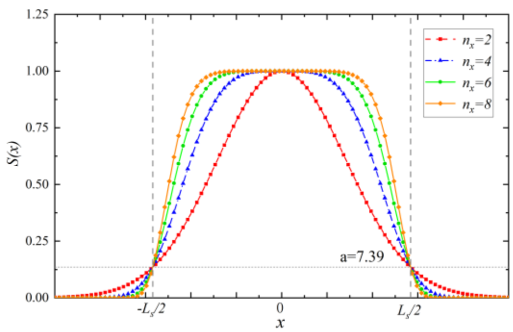

Fig. 2 A comparison of the pressure distribution profiles corresponding to different exponential factors while maintaining a constant decay coefficient $a = 7.39$ (configuration 2).

Fig. 3 presents the pressure distributions for $n_x = 4$ with varying values of a . The observed trends align with the parametric dependencies illustrated in Fig. 1 and Fig. 2, showing consistent behavior in the evolution of the pressure profile morphology. In accordance with the established patterns, further elaboration is omitted here to maintain conciseness.

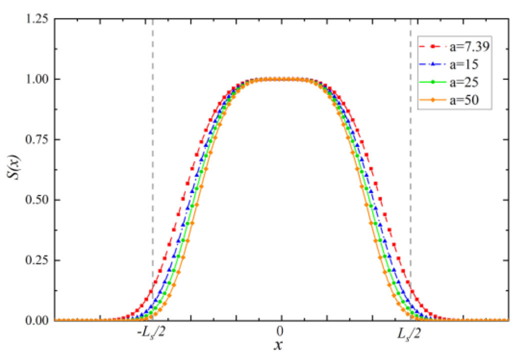

Fig. 3 Comparison of pressure distribution under configuration 3.

Using the DTMB 5415 as the reference hull form—with a length of 142.0 m, beam of 18.9 m, and draft of 6.16 m—the shape of the pressure distribution function is determined via Eq. (12). For simplicity, this study confines the discussion to cases where identical decay coefficients and exponential factors are applied at the bow, stern, and sides. Hereafter, the symbols β (equivalently, a) and n are used to denote these unified parameters. The three-dimensional morphology of the Gaussian pressure distribution is visualized in Fig. 4 to Fig. 7 through the shape factor $S(x, y)$ for four parametric configurations. These representations exhibit evolutionary patterns consistent with the earlier quantitative analysis. No detailed description is repeated here in keeping with the systematic presentation of results.

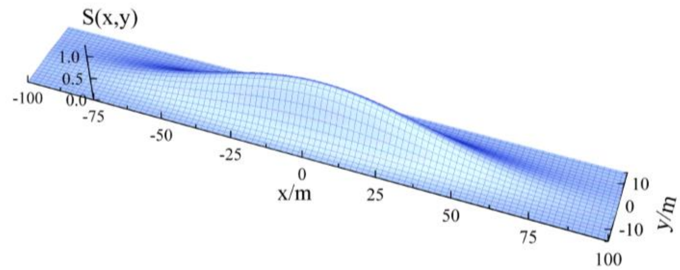

Fig. 4 3d graph of $S(x, y)$: $a = 7.39$ and $n = 2$.

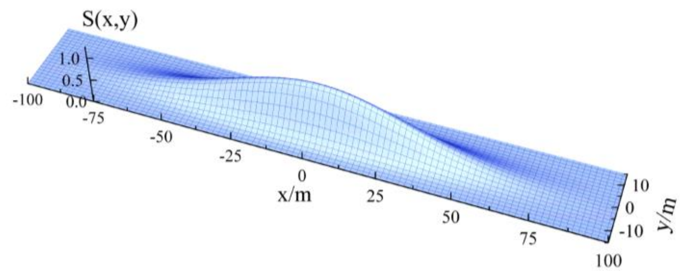

Fig. 5 3d graph of $S(x, y)$: $a = 15$ and $n = 2$.

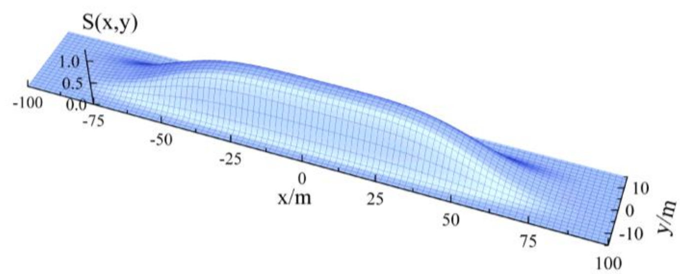

Fig. 6 3d graph of $S(x, y)$: $a = 7.39$ and $n = 4$.

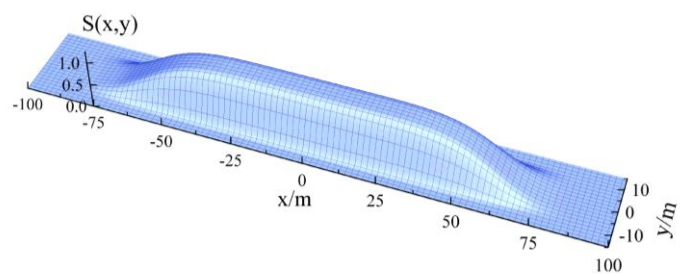

Fig. 7 3d graph of $S(x, y)$: $a = 7.39$ and $n = 6$.

Kelvin Wakes with Different Pressure Distributions

Numerical simulations were conducted for Configurations 1 and 2 specified in Tab. 1. The significant wave period Tp_{real} was set to 10 s in HOS-Ocean for wave field initialization. All cases employed a dimensionless computational domain of $xlen = 20$ and $ylen = 10$, corresponding to approximately $3120\,m \times 1560\,m$ in physical scale. The grid resolution was maintained at $n_1 = 256$ and $n_2 = 128$ nodes in the longitudinal and transverse directions, respectively. The simulation duration was set to $T_{stop} = 30$ (equivalent to 300 s in prototype scale). The computations were performed on a 3.60 GHz Intel Core i7-9700 single-core processor, with a total computational time of approximately

36 minutes, demonstrating high computational efficiency.

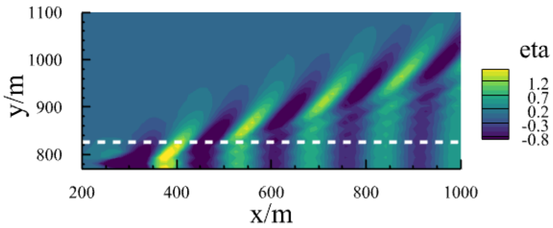

Fig. 8 The wave field predicted by the Gaussian pressure distribution.

As shown in Fig. 8, the Kelvin wake pattern computed using the standard Gaussian pressure distribution ($a = 7.39$, $n = 2$) is presented. To quantitatively validate the results, the free-surface elevation η was sampled along the transverse plane at $y' = 46\ m$ (indicated by the white dashed line) and compared against Lindenmuth's (1991) reference data. This specific cross-section ($y' = 46\ m$) serves as the standardized location for all comparative analyses of wave elevation data across different numerical cases in this investigation.

Fig. 9 and Fig. 10 illustrate the influence of different decay coefficients β (expressed via the equivalent peak factor a) on the resulting Kelvin wake structure. While the far-field wave patterns obtained with the standard Gaussian pressure distribution show reasonable agreement with reference data, notable discrepancies emerge in the near-field region. Specifically, the first peak amplitude is significantly underestimated in the simulation. This discrepancy may be attributed to the overly smooth bow-stern transition in the standard Gaussian representation, which fails to capture the abrupt geometrical changes typical of actual ship hulls.

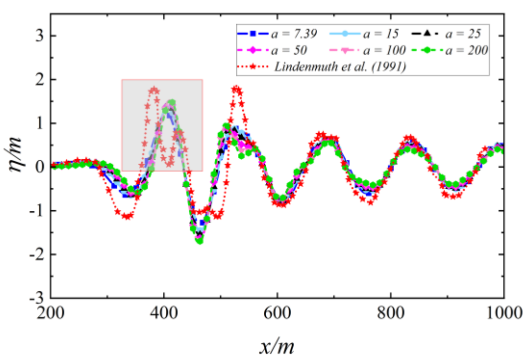

Fig. 9 Results and comparison for configuration 1.

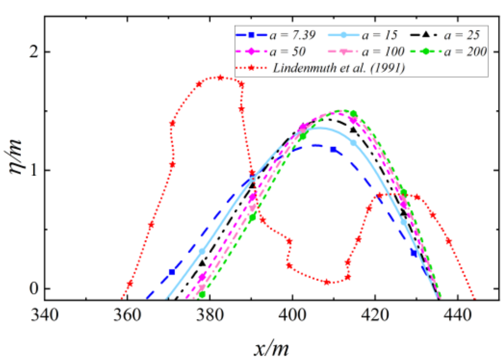

Fig. 10 The shaded area from Fig. 9.

To investigate this phenomenon, extreme values of the decay coefficient were examined. However, even substantially increased a values yielded negligible improvement in wake prediction accuracy. Although insufficient grid resolution for capturing steep pressure gradients could theoretically contribute to this limitation, the analysis suggests this is not the primary factor. A more plausible explanation lies in the fundamental structure of the Gaussian distribution itself: its concentration around a single peak effectively creates only one dominant wave-making source, unlike actual ship hulls which generate independent wave systems from both bow and stern. This fundamental difference explains why field measurements typically show two distinct peaks in the first crest region, while the standard Gaussian model produces only one.

Based on these observations, it was noted that increasing the exponential factor n in the pressure distribution could potentially better represent this characteristic. Therefore, Kelvin wake patterns under different n values (Configuration 2) were investigated, with results shown in Fig. 11 and Fig. 12. Comparative analysis reveals that the improved Gaussian pressure distribution maintains good agreement in far-field wave elevation while demonstrating notable improvement in near-field predictions.

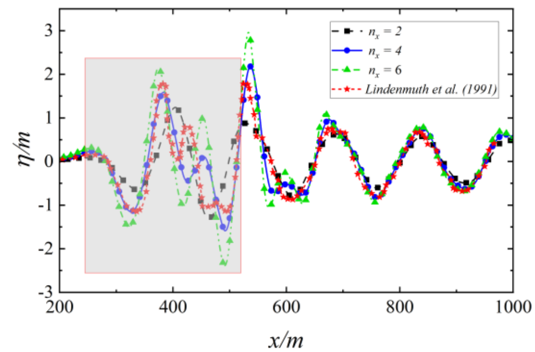

Fig. 11 Results and comparison for configuration 2.

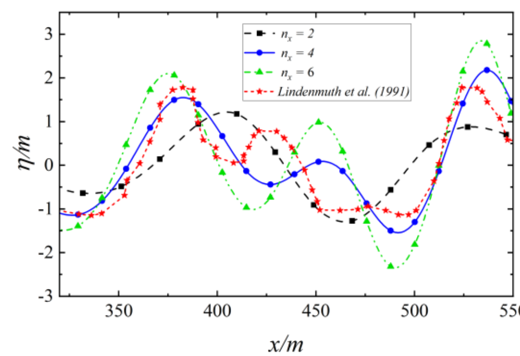

Fig. 12 The shaded area from Fig. 11.

Specifically, two key improvements are observed compared to the standard Gaussian distribution: first, better agreement is achieved at the first wave trough; second, dual crests emerge near the second wave peak while maintaining comparable amplitude characteristics. This morphological enhancement confirms that the box-like pressure distribution resulting from increased n values effectively represents the dual wave-making sources at bow and stern regions. Although positional discrepancies persist between these dual crests, further refinement through coordinated adjustment of both decay coefficient β and exponential factor n may provide necessary control over the spatial distribution of these wave-making sources.

Fig. 13 to Fig. 16 present the free-surface contours of Kelvin wakes generated by Gaussian pressure distributions with different parameter configurations. At this Froude number, the wave system consists of both transverse and divergent waves, with both components being clearly visible.

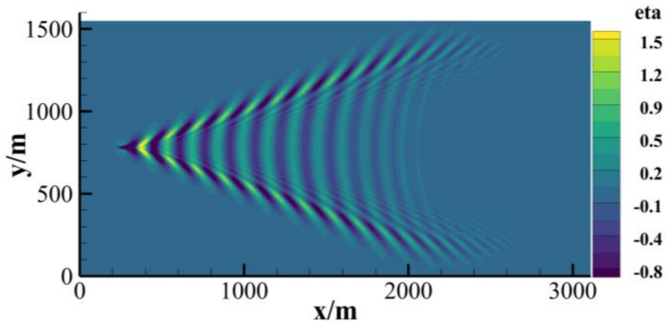

Fig. 13 Kelvin wake: $a = 7.39$ and $n = 2$.

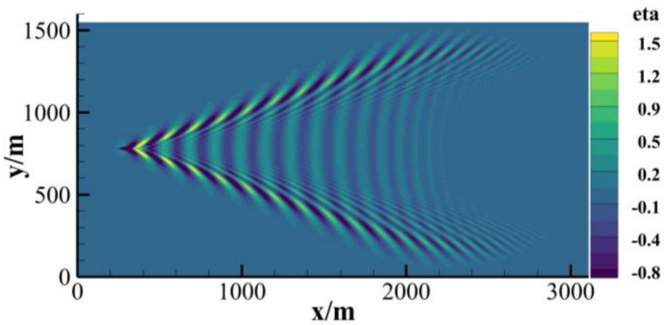

Fig. 14 Kelvin wake: $a = 200$ and $n = 2$.

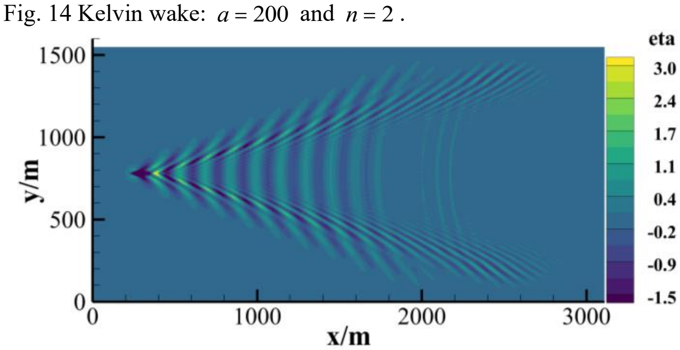

Fig. 15 Kelvin wake: $a = 7.39$ and $n = 4$.

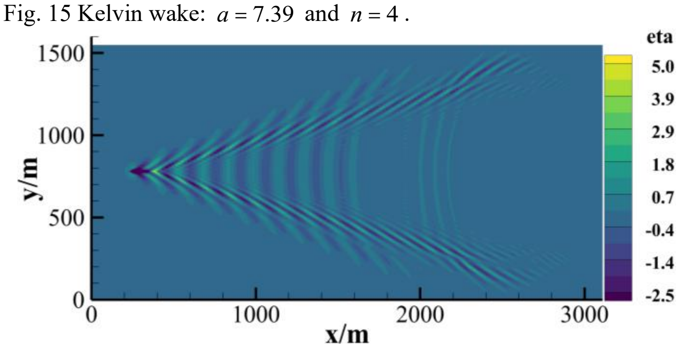

Fig. 16 Kelvin wake: $a = 7.39$ and $n = 6$.

Analysis reveals that varying the value of a while maintaining a constant n produces minimal alteration to the overall wake structure. In contrast, when a remains fixed and n increases from 2 to 4, significant modifications occur in the Kelvin wake pattern. Specifically, the modified distribution generates a bow wave system that is absent in the standard Gaussian model ($n = 2$). However, further increasing n beyond 4 yields diminishing returns in terms of structural changes to the wake system.

This behavior can be attributed to the relative sensitivity of the pressure distribution to parameter variations. While adjustments to a primarily affect the distribution's decay rate, the exponential factor n directly controls the fundamental shape characteristics. The observed saturation effect with increasing n values suggest the existence of a threshold beyond which additional shape modifications become marginal.

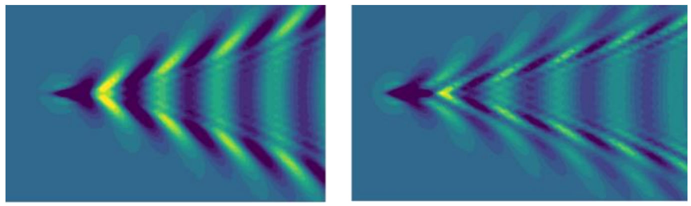

(a) $a = 7.39$, $n = 2$ (b) $a = 7.39$, $n = 4$

Fig. 17 Wave system generated by pressure distribution.

Fig. 17 provides a comparative visualization of the relationship between Gaussian pressure distributions and their corresponding Kelvin wake systems for $n = 2$ and $n = 4$. In the standard Gaussian distribution ($n = 2$), wave-making primarily originates from the central region of the pressure distribution, corresponding to the peak pressure area, without generating a secondary wave system. In contrast, the improved Gaussian distribution ($n = 4$) clearly produces two distinct wave systems originating from positions ahead of and behind the pressure distribution midportion. This phenomenon directly relates to the box-like pressure distribution characteristics resulting from the increased exponential factor n , where pressure concentration shifts from being predominantly central to being distributed at both forward and aft sections.

CONCLUSIONS

An improved pressure distribution model was developed based on the standard Gaussian formulation to better represent hull geometry features such as the parallel middle body, thereby enabling improved simulation of hull-induced free-surface disturbances. The shape control parameters a and n jointly determine the shape represented by the pressure distribution term, thereby leading to different Kelvin wake patterns. The proposed model was implemented within the open-source solver HOS-Ocean using the High-Order Spectral method, allowing numerical simulation of Kelvin wake generation and evolution in open-water conditions.

For the DTMB 5415 considered as the reference hull form in this study, with a length of 142.0 m, a beam of 18.9 m, and a draft of 6.16 m, reasonably satisfactory results can be obtained when $a = 7.39$ and $n = 4$. Comparative results demonstrate that the improved pressure distribution maintains far-field wave elevation accuracy while successfully generating both bow and stern wave systems. Significantly improved agreement with reference data was observed in near-field surface elevation predictions. This work provides an enhanced computational framework for Kelvin wake simulation and establishes a foundation for further investigation of ship-generated wave patterns.

ACKNOWLEDGEMENTS

This work was supported by the National Natural Science Foundation of

China (52571359, 52131102), to which the authors are most grateful.

APPENDIXE A.

For the distribution function described by Eq. (7), it can be shown that, given the target hull dimensions L_s and B_s, when the peak value is taken as $1/a$, the standard deviations σ_x and σ_y satisfy the relationship with the hull dimensions given by Eq. (8). This is equivalent to stating that if the condition is imposed such that the contour where the shape function $S(x,y)$ takes the value $1/a$ corresponds precisely to the spatial extent of the hull, then the relation given by Eq. (8) holds. And then:

$$S(x,y) = \exp(-\frac{1}{2}\left[\frac{(x-\mu_x)^n}{\sigma_x^n} + \frac{(y-\mu_y)^n}{\sigma_y^n}\right]) = \frac{1}{a} \quad (15)$$

Taking the logarithm of both sides, Eq. (15) then becomes:

$$\frac{(x-\mu_x)^n}{\sigma_x^n} + \frac{(y-\mu_y)^n}{\sigma_y^n} = 2\ln(a) \quad (16)$$

Eq. (16) resembles the standard form of an ellipse, and its further transformation yields:

$$\frac{(x-\mu_x)^n}{(\sigma_x \cdot (2\ln(a))^{1/n})^n} + \frac{(y-\mu_y)^n}{(\sigma_y \cdot (2\ln(a))^{1/n})^n} = 1 \quad (17)$$

Clearly, this contour represents an ellipse-like shape. If its semi-major and semi-minor axes are set equal to the ship length L_s and ship width B_s, respectively, then:

$$2\sigma_x \cdot (2\ln(a))^{1/n} = L_s, \quad 2\sigma_y \cdot (2\ln(a))^{1/n} = B_s \quad (18)$$

A straightforward manipulation of the above expression yields the relationship shown in Eq. (8).

$$\sigma_x = \frac{L_s/2}{(2\ln(a))^{1/n}}, \qquad \sigma_y = \frac{B_s/2}{(2\ln(a))^{1/n}} \quad (19)$$

ACKNOWLEDGEMENTS

This work was supported by the National Key Research and Development Program of China (2025YFF0519800), to which the authors are most grateful.

REFERENCES

Arnold-Bos, A, Martin, A, and Khenchaf, A (2007). "Obtaining a ship's speed and direction from its Kelvin wake spectrum using stochastic matched filtering," *In 2007 IEEE International Geoscience and Remote Sensing Symposium*, IEEE, 1106-1109.

Bao, P, Ren, M, Huang, F, Wan, D, and Zhuang, Y (2025). "Numerical simulation of wide-area Kelvin's ship wake based on high-order spectral method," *Physics of Fluids*, 37(12).

Colen, J, and Kolomeisky, EB (2021). "Kelvin–Froude wake patterns of a traveling pressure disturbance," *European Journal of Mechanics-B/Fluids*, 85, 400-412.

Dommermuth, DG, and Yue, DK (1987). "A high-order spectral method for the study of nonlinear gravity waves," *Journal of Fluid Mechanics*, 184, 267-288.

Ducrozet, G, Bonnefoy, F, Le Touzé, D, and Ferrant, P (2016). "HOS-ocean: Open-source solver for nonlinear waves in open ocean based on High-Order Spectral method," *Computer Physics Communications*, 203, 245-254.

Gomit, G, Rousseaux, G, Chatellier, L, Calluaud, D, & David, L (2014). "Spectral analysis of ship waves in deep water from accurate measurements of the free surface elevation by optical methods," *Physics of Fluids*, 26(12).

Graziano, MD, D'Errico, M, and Rufino, G (2016). "Ship heading and velocity analysis by wake detection in SAR images," *Acta astronautica*, 128, 72-82.

Lindenmuth, W, Ratcliffe, TJ, and Reed, AM (1991). "Comparative Accuracy of Numerical Kelvin Wake Code Predictions-'Wake Off'," (No. DTRC91004).

Lo, PHY (2021). "Approximate ship wake solution for fast computation," *Ocean Engineering*, 235, 109405.

Moisy, F, and Rabaud, M (2014). "Scaling of far-field wake angle of nonaxisymmetric pressure disturbance," *Physical Review E*, 89(6), 063004.

Paprota, M (2023). "A Fourier Galerkin method for ship waves," *Ocean Engineering*, 271, 113796.

Rabaud, M, and Moisy, F (2013). "Ship wakes: Kelvin or Mach angle?," *Physical review letters*, 110(21), 214503.

Sun, YX, Liu, P, and Jin, YQ (2018). "Ship wake components: Isolation, reconstruction, and characteristics analysis in spectral, spatial, and TerraSAR-X image domains," *IEEE Transactions on Geoscience and Remote Sensing*, 56(7), 4209-4224.

Tunaley, JK (2003). "The estimation of ship velocity from SAR imagery," In IGARSS 2003. 2003 *IEEE International Geoscience and Remote Sensing Symposium*, IEEE, 1,191-193.

Yeung, RW, and Wan, H, Banumurthy, SP, Ham, WL, and Lew, JM (2008). "Effects of configuration on wave resistance of multiple pressure distributions," *Marine Systems & Ocean Technology*, 4(2), 53-62.

Zakharov, VE (1968). "Stability of periodic waves of finite amplitude on the surface of a deep fluid," *Journal of Applied Mechanics and Technical Physics*, 9(2), 190-194.